# Retrieving internal wave surface currents from SAR image

FAN Kai-guo[1,2,3], HUANG Wei-gen[1], GAN Xi-lin[1], FU Bin[1]

1. *State Key Laboratory of Satellite Ocean Environment Dynamics, Second Institute of Oceanography, State Oceanic Administration, Zhejiang Hangzhou* 310012, *China*;
2. *Institute of Space and Earth Information Science, The Chinese University of Hong Kong, Hong Kong, China*;
3. *Key Laboratory of Ocean Remote Sensing, Ministry of Education, Ocean University of China, Shandong Qingdao* 266003, *China*

**Abstract:** Based on ocean internal wave Synthetic Aperture Radar (SAR) imaging mechanism and the M4S model, which was applied to simulate the oceanic features of ocean surface, one new method for retrieving internal wave surface currents from SAR image is introduced. Firstly, according to the AH linear theory, the first guessed surface currents could be estimated from the normalized radar crossing section (NRCS) of the internal wave profile in SAR image, and the signal induced by internal wave surface currents can be simulated by M4S. Then the wind speed and internal wave surface currents gradients are modified using the dichotomy method step by step, which causes the simulated signal close to the NRCS measured from SAR image. Finally, the wind speed and the surface currents could be retrieved until a satisfied match between the simulated signals and SAR images. This method is tested on three ERS-2 SAR images in the South China Sea. The results show that the simulated internal wave signal is consistent with the NRCS of internal wave SAR images. Their correlation coefficients are up to 90%, which indicate that this method is convergent and applicable.

**Key words:** SAR, internal wave, surface currents, retrieval

**CLC number:** P71/TP722.6 **Document code:** A

**Citation format:** Fan K G, Huang W G, Gan X L and Fu B. 2010. Retrieving internal wave surface currents from SAR image. *Journal of Remote Sensing*. **14**(1): 122—130

## 1 INTRODUCTION

Ocean internal waves are meso-scale phenomenon that travel within the interior ocean and change the ocean surface roughness. As synthetic aperture radar (SAR) works in microwave and resonates with surface Bragg waves, so SAR has the ability of observing ocean internal waves and this has been realized for some time. And the ocean internal waves appear as elongated bright and dark features in SAR images, due to the interaction between the surface Bragg waves and the surface currents induced by the spatially varying ocean internal waves (Alpers, 1985). Also since SAR can provide all-weather, day-night images of the ocean surface with a wider swath and a higher spatial resolution, therefore, intensively investigations and efforts have been made to the ocean internal waves study by SAR.

Ocean internal waves have the large amplitude waves existing in the pycnocline. During its propagation process, the induced disturbance can bring about strong convergence of sea water and sudden strong currents, which can cause severe threat to the ocean engineering structures, such as oil drilling platforms and pipelines (Cai *et al.*, 2003). Also, the surface currents knowledge is very crucial for retrieving valuable information about internal wave amplitude, undisturbed upper layer thickness, propagation direction, and relative density difference (Brandt *et al.*, 1999). Especially, the surface currents knowledge could provide the information for study internal wave evolution as they propagation away from their generation regions (David, 1999). Therefore it is adequate for quantitative estimates of internal wave surface currents from SAR images, and is also especially significant in SAR technique for internal wave research.

Brandt (1999) has studied the feasibility of retrieving ocean internal wave parameters from the normalized radar crossing section (NRCS) of internal wave profile in SAR images. David (1999) has extracted the ocean internal wave peak surface currents information through the simulated signals and the NRCS from SAR images, and results indicate that the peak surface currents estimates are within 15% of the observed *in situ* data. Both above methods have the crucial request for the radar microwave scattering imaging model for ocean surface. However, there is little focus on the study of the internal wave surface currents information retrieval from SAR image in China. So the study of the internal wave surface currents retrieval from SAR image, combing with the radar microwave scattering imaging model and the NRCS of internal waves profile in SAR image, is still in the exploratory step.

In this paper, one new inversion method for retrieving internal wave surface currents from SAR image has been developed. This method is based on iterative fitting of SAR image by the forward radar microwave scattering imaging simulating, which is combined by wave-current interaction, radar scattering and

**Received**: 2008-08-22; **Accepted**: 2008-11-18

**First author biography**: FAN Kai-guo (1981— ), male. He received the PH. D. degree from Ocean University of China, Qingdao, in 2009. His interests are in physical oceanography and satellite ocean, atmospheric remote sensing. He has published more than 15 papers. E-mail: van.fkg@tom.com

ocean internal wave SAR imaging theory. Its applications to three ERS-2 SAR images in the South China Sea, and their correlation coefficients of both the simulated internal wave signals and the NRCS in SAR image show that the inversion method is convergent and applicable.

## 2 INTERNAL WAVE SAR IMAGING MECHANISM

SAR cannot directly view ocean internal waves, and the radar waves can only penetrate seawater in a centimeters degree. However, by convergence and divergence modulation effect, internal waves will modulate ocean surface micro-scale waves, which will in turn modulate the backscattered radar signals. In this way, SAR captures rich information about internal waves under favorable meteorological conditions (wind conditions 2—9m/s) (Alpers, 1985; Thomson & Gasparovic, 1986).

An extensive study of ocean internal waves SAR imaging physical mechanisms was conducted, and it is generally accepted that the imaging mechanism of observing internal waves by SAR is the hydrodynamics modulation theory, which consists of three stages (Alpers & Hennings, 1984; Alpers, 1985; Thomson & Gasparovic, 1986).

Firstly, the propagation of ocean internal waves results in the modulation of surface flow velocity. Secondly, the modulation by surface flow velocity causes variations of the surface wave spectrum. Finally the variation of the surface spectrum causes modulation in the level of radar backscatter. Based on above three stages, ocean internal waves are imaged by SAR.

## 3 M4S MODEL FOR RADAR MICROWAVE IMAGING OCEAN SURFACE

Combining the Wentzel-Kramers-Brillouin weak hydrodynamic interaction theory, which described by the equation of wave action balance, and the radar microwave scattering model, Dr. Romeiser from the University of Hamburg has been developed an advanced forward M4S model. This model can forward simulate the oceanic features over the ocean surface likely spatially varying surface currents of ocean internal waves via hydrodynamic modulation (Romeiser & Alpers, 1997).

M4S model is a software toolkit for numerical simulations of ocean surface and it is divided into two components: wave-current interaction and radar microwave scattering imaging. For the wave-current interaction, the modulated surface wave spectra are computed from the equation of wave action balance by ray tracing, and the radar microwave backscatter imaging is computed from the improved composted surface model.

### 3.1 Equation of wave action balance

The equation of wave action balance describes the evolution of the energy of a wave packet that travels trough a slowly varying surface current field (Alpers, 1984; Romeiser & Alpers, 1997) and reads

$$\frac{dA}{dt}=\frac{\partial\Omega}{\partial k_x}\frac{\partial A}{\partial x}+\frac{\partial\Omega}{\partial k_y}\frac{\partial A}{\partial y}-\frac{\partial\Omega}{\partial x}\frac{\partial A}{\partial k_x}-\frac{\partial\Omega}{\partial y}\frac{\partial A}{\partial k_y}=S \qquad (1)$$

where $A(\boldsymbol{r}, \boldsymbol{k}, t)$ is the action spectral density of the wave packet, $\Omega(\boldsymbol{r}, \boldsymbol{k}, t)$ the apparent frequency in the moving medium, $\boldsymbol{r} = (x, y)$ the parameters of the space, $\boldsymbol{k}=(k_x, k_y)$ the wave number vectors of the wave packet and $S(\boldsymbol{r}, \boldsymbol{k}, t)$ a source function.

In the M4S source code, the spatially varying wave spectra were further computed by numerical integration the equation of wave action balance through ray-tracing method.

### 3.2 Radar microwave scattering model

An improved composted surface model for calculation NRCS calculation of the ocean surface is developed by Dr. R. Romeiser and Prof. W. Alpers. Also, this can be called "three-scale model", because there are Bragg waves, all longer waves, and usually a modulating feature such as internal wave current gradients, which modulate all the ocean surface short waves. The model yields comparable radar signatures in the presence of the spatially varying surface currents, and is much better in agreement with the experimental results. It was believed that the improved composted surface model has good potential for incorporation into inversion models for the determination of the surface currents fields from SAR images (Romeiser *et al.*, 1994; Romeiser & Alpers, 1997).

In the M4S source code, radar signatures in the presence of spatially varying surface currents would be calculated by combing with the wave spectra, which were computed from the equation of wave action balance, and the radar parameters inputted.

## 4 SAR INVERSION MODEL

Alpers and Hennings has concluded that the relative NRCS of internal wave SAR images was linear proportional to the surface currents gradients, and the AH linear theory can be read (Hughes 1978; Alpers & Hennings, 1984; Alpers, 1985).

$$\frac{\Delta\sigma^0}{\sigma_0^0}=-A\cos^2\phi\frac{\partial U_x}{\partial x}=-C\frac{\partial U_x}{\partial x} \qquad (2)$$

where $\Delta\sigma^0=\sigma^0-\sigma_0^0$, $\sigma^0$ is the NRCS of ocean surface, $\sigma_0^0$ is the NRCS of sea surface background, $A$ is a coefficient related to the wind speed and wind direction, $\phi$ is the relative angle between the internal wave propagation direction and radar direction, $C=A\cos^2\phi$.

The inversion model starts with an initial guess set of parameters. According to Eq.(2), the relative NRCS of internal wave profile in SAR images is linear proportional to the surface currents gradients, so the first guessed surface currents could be estimated from the NRCS of ocean internal wave profile. Here the initial mean current speed is given by the current model. Radar parameters and initial wind information obtained from the national centers for environmental prediction (NCEP) reanalysis wind data are also fixed inputs the M4S model, then the signals induced by the oceanic internal wave can be simulated.

The wind speed and the internal wave surface currents gradients are modified using the dichotomy method step by step, which means refinement of the estimates is done at each iteration until the best match achieved between SAR image signal observations and M4S model simulated results. Finally, the wind speed and the surface currents can be retrieved, and also the final parametric values are then the best-fit surface currents and wind parameters. During this procedure, the right chosen initial wind speed and the coefficient of velocity gradient will speed up the convergence rate of iterative simulation.

Fig. 1 gives the flowchart of ocean internal wave surface currents retrieved from SAR image based on M4S model.

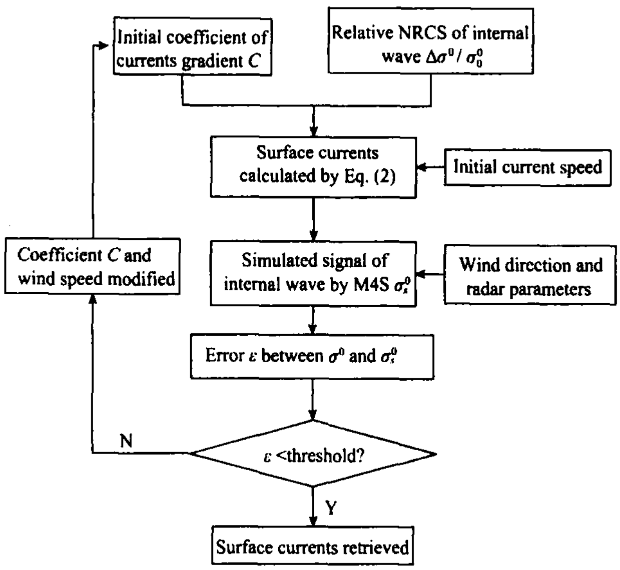


Fig. 1 Flowchart of internal wave surface currents retrieved from SAR image based on M4S

## 5 SAR INVERSION RESULTS

### 5.1 Case one

Fig.2 (a) shows the ERS-2 SAR image with ocean internal wave features of elongated bright and dark features in the north-west area of Pratas Island. It was acquired at 10:00 on October 2, 2000 (BJT). The pixel size of the image is about 12.5 m and the radar wavelength is 5.66 cm. The data line *A-B* taken from Fig.2 (a) represents the NRCS profile of the internal wave SAR image, which is the solid line in Fig.2 (b).

The initial guess set of parameters such as local wind direction and speed in this area could be obtained from NCEP reanalysis wind data, also the wind speed could be retrieved from SAR image. The initial values of the surface current gradients and ocean internal wave surface currents could be estimated by Eq.(2).

In the line data *A-B* iterative inversion, the initial wind direction at the imaging time is about 68.46° and based on daily averaged NCEP reanalysis wind data the wind speed is about 2.77m/s. The coefficient of currents gradient *C* related to the wind speed and wind direction estimated is about 0.0007. Parameters related with the radar are known, e.g., the incidence angle of radar is 20.15° and then fixed inputs the M4S model.

After 17 iteration steps, the final wind speed is 1.29m/s and the coefficient of currents gradient *C* is 0.000282 respectively. The retrieved internal wave surface currents is also seen in Fig.2 (c). Here, both the simulated signal of internal wave, which is the dashed line in Fig.2 (b), and the NRCS in SAR image has the correlation coefficient 92.3%, indicating the ocean internal wave simulated signals compared favorably with the observed NRCS in SAR images and this inversion method is convergent and applicable.

### 5.2 Case two

Fig.3 (a) also shows the ERS-2 SAR image with ocean internal wave features in the near area of Pratas Island. It was acquired at 22:00 on June 23, 1998 (BJT). The pixel size of the image is about 12.5 m, the radar wavelength is 5.66 cm and incidence angle of radar is about 21.65°. Also, the data line *M-N* taken from Fig.3 (a) represents the profile of the internal wave SAR images, which is the solid line in Fig.3 (b).

In the line data *M-N* iterative inversion, the initial wind direction at the imaging time is about 150.75° and the wind speed is about 1.98m/s, but the coefficient of currents gradient *C* is initially fixed as 0.0007.

After 10 iteration steps, the final wind speed is 2.15m/s and the coefficient of currents gradient *C* become 0.000888. The retrieved internal wave surface currents is seen in Fig.3 (c). Here, the simulated signal of internal wave, which is the dashed line in Fig.3 (b), and the NRCS in SAR images has the correlation coefficient 93.8%. This result further validates that this method of retrieving internal wave surface currents from SAR image is convergent and applicable.

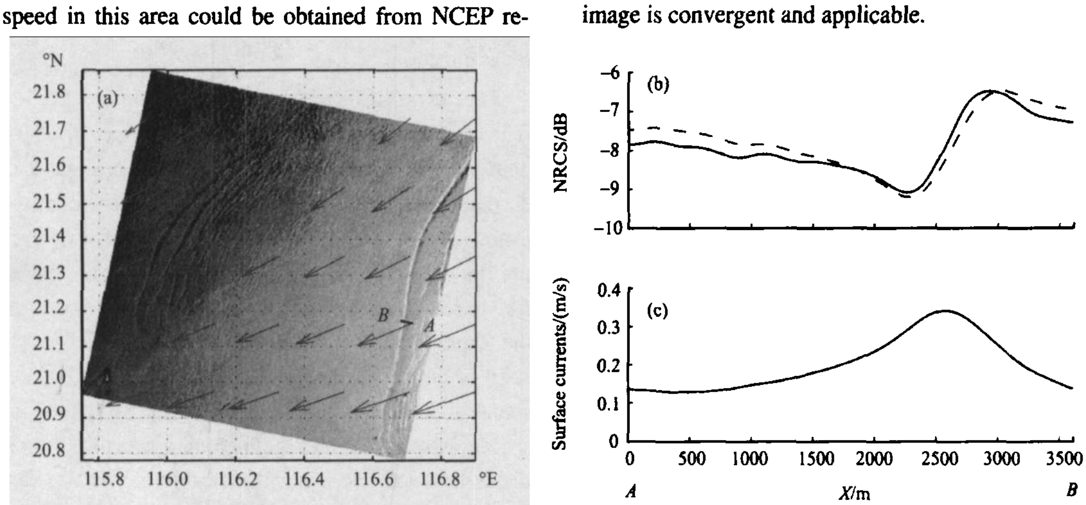


Fig. 2 (a) ERS-2 SAR images obtained at Oct. 2, 2000 and the NCEP wind field; (b) The profile of internal wave SAR image (solid line) and simulated (dashed line); (c) Internal wave surface currents retrieved from SAR image

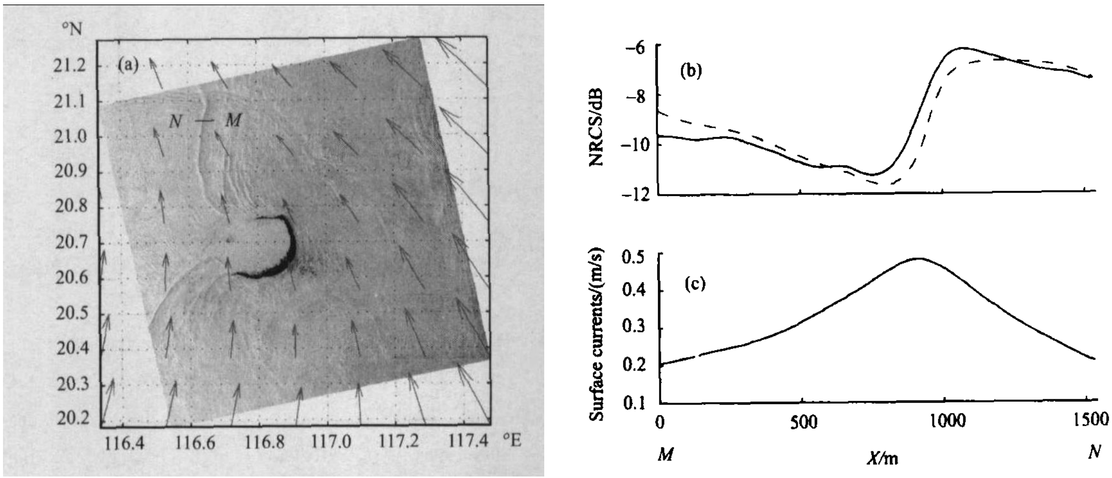


Fig. 3 (a) ERS-2 SAR images obtained at 23 Jun. 1998 and the NCEP wind field; (b) The profile of internal wave SAR image (real line) and simulated (dashed line); (c) Internal wave surface currents retrieved from SAR image

### 5.3 Case three

Fig.4 (a) shows the ocean internal wave ERS-2 SAR image, which was acquired at 22:00 on April 22, 1998 (BJT). The data line *P-Q* taken from Fig.4 (a) represents the profile of the internal wave SAR images, which is the solid line in Fig.4 (b).

In the line data *P-Q* iterative inversion, the initial wind direction is about 149.67° and the initial wind speed is about 2.36m/s based on daily averaged NCEP reanalysis wind data, and the initial coefficient of currents gradient *C* is also fixed as 0.0007. The incidence angle of radar is 26.35° and other parameters related with the radar are fixed inputs the M4S model.

After 15 iteration steps, the final wind speed 1.92m/s and the coefficient of currents gradient *C* 0.000356 were calculated. The retrieved internal wave surface currents is also seen in Fig.4 (c). Here, the simulated signal of internal wave, which is the dashed line in Fig.4 (b), and the NRCS in SAR images has the correlation coefficient 95.8%, which is much better than the correlation coefficient of the two previous cases.

## 6 CONCLUSIONS

Method for retrieving internal wave surface currents from SAR image is introduced based on the ocean internal wave SAR imaging mechanism and M4S model. The convergence and applibility of this method are tested by correlation coefficient between both the simulated signals and internal waves SAR images.

Its applications to three ERS-2 SAR images indicate that, despite having some differences between the internal wave SAR images and simulated signal at the last inversion iteration, the simulated internal wave signal is consistent with the internal wave SAR image. The correlation coefficients are up to 90%, which mean that this method is convergent and applicable. Therefore the accurate surface currents of internal waves can be obtained from SAR images. This measure can be applied to any internal wave case under any stratification and any water depth without assuming the dynamical model of the ocean internal waves.

**Acknowledgements:** The authors would like to thank Dr. Romeiser for providing M4S model, Remote Sensing Ground Station of China, Chinese Academy of Sciences (CAS) and European Space Agency (ESA) for providing SAR images, the Institute of Atmospheric Physics, CAS for providing the national center for environmental prediction (NCEP) reanalysis wind data.

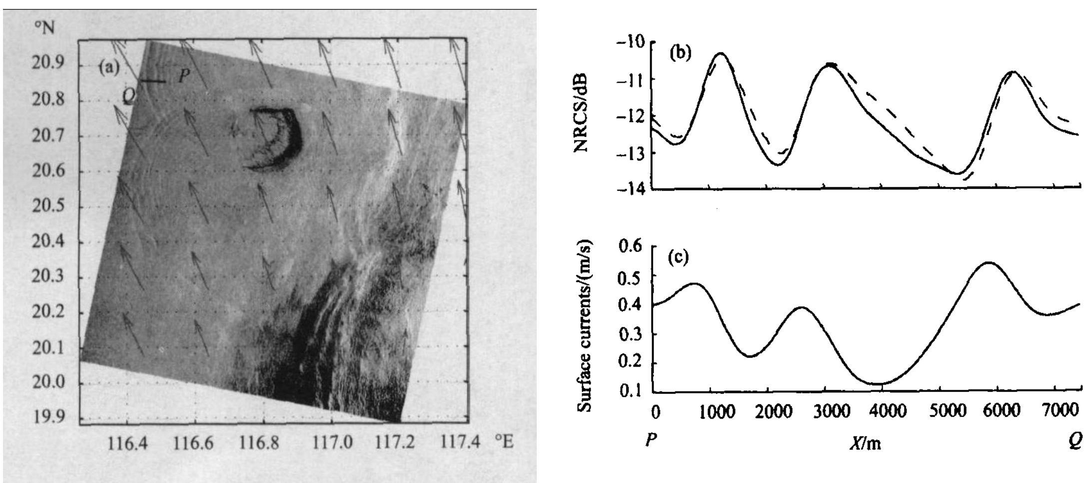


Fig. 4 (a) ERS-2 SAR images obtained at 22 Apr. 1998 and the NCEP wind field; (b) the profile of internal wave SAR image (real line) and simulated (dashed line); (c) internal wave surface currents retrieved from SAR image

## REFERENCES

Alpers W and Hennings I. 1984. A theory of the imaging mechanism of underwater bottom topography by real and synthetic aperture radar. *Journal of Geophysical Research*, **89**: 10529—10546

Alpers W. 1985. Theory of radar imaging of internal waves. *Nature*, **314**: 245—247

Brandt P, Romeiser R and Rubino A. 1999. On the determination of characteristics of the interior ocean dynamics from radar signatures of internal solitary waves. *Journal of Geophysical Research*, **104**(C12): 30039—30045

Cai S Q, Long X M and Gan Z J. 2003. A method to estimate the forces exerted by internal solitons on cylindrical piles. *Ocean Engineering*, **30**: 673—689

David Y L. 1999. Extraction of surface currents of solitary internal waves from synthetic aperture radar data. Proceedings of the IEEE Sixth Working Conference on Current Measurement. San Diego: IEEE

Hughes B A. 1978. The effect of internal waves on surface wind waves 2. Theoretical analysis. *Journal of Geophysical Research*, **102**: 1163—1181

Romeiser R and Alpers W. 1997. An improved composite surface model for the radar backscattering cross section of the ocean surface 1. Theory of the model and optimization/validation by scatterometer Data. *Journal of Geophysical Research*, **102**: 25238—25250

Romeiser R and Alpers W. 1997. An improved composite surface model for the radar backscattering cross section of the ocean surface 2. Model response to surface roughness variations and the radar imaging of underwater bottom topography. *Journal of Geophysical Research*, **102**(C11): 25 251—25 267

Romeiser R, Schnidt A and Alpers W. 1994. A three-scale composite surface model for the ocean wave-radar modulation transfer function. *Journal of Geophysical Research*, **99**(C5): 9785—9801

Thomson R E and Gasparovic R F. 1986. Intensity modulation in SAR image of internal waves. *Nature*, **320**(14): 345—348

# SAR 海洋内波表层流反演方法探讨

范开国[1,2,3], 黄韦艮[1], 甘锡林[1], 傅　斌[1]

1. 国家海洋局 第二海洋研究所, 卫星海洋环境动力学国家重点实验室, 浙江 杭州　310012;
2. 香港中文大学 太空与地球信息科学研究所, 香港;
3. 中国海洋大学 海洋遥感教育部重点实验室, 山东 青岛　266003

**摘　要**: 基于海洋内波 SAR 成像机理与 M4S 海面微波散射成像模型, 提出 SAR 海洋内波表层流反演新方法。首先从 SAR 图像上获得内波剖面的海面后向散射强度, 利用 AH 理论的线性近似关系得到猜测表层流, 通过海面微波散射成像模型仿真海洋内波的 SAR 海面后向散射强度, 利用二分法不断地修改风速和流速梯度等参数, 使仿真信号最大程度的逼近实际SAR图像上的海面后向散射强度, 输出最终海表层流。以中国南海海区 3 景海洋内波 SAR 图像为例, 对该方法进行了探讨。结果表明, 仿真的海洋内波 SAR 海面后向散射强度剖面和实际 SAR 图像上的信号剖面吻合, 两者的相关系数达 90%以上, 说明该反演方法是收敛与可行的。

**关键词**: 合成孔径雷达, 海洋内波, 表层流, 反演

**中图分类号**: P71/TP722.6　　**文献标识码**: A

**引用格式**: 范开国, 黄韦艮, 甘锡林, 傅　斌. 2010. SAR 海洋内波表层流反演方法探讨. 遥感学报, 14(1): 122—130
Fan K G, Huang W G, Gan X L and Fu B. 2010. Retrieving internal wave surface currents from SAR image. *Journal of Remote Sensing*. 14(1): 122—130

## 1 引　言

海洋内波是一种发生在海洋内部的中尺度现象。海洋内波引起海面表层流辐聚或辐散, 改变了海面粗糙度, 通过 Bragg 共振散射作用, 在全天时、全天候、高分辨率合成孔径雷达(Synthetic Aperture Radar, SAR)图像上形成明暗相间的条纹(Alpers, 1985)。

海洋内波携带的巨大能量会导致异常强大的流速, 对海洋工程、石油钻井平台和海底石油管道造成严重的威胁(Cai 等, 2003)。高分辨率海洋内波表层流信息的获取为开展从SAR图像上获取更为准确的内波波长、方向、振幅与混合层深度等内波参数有重要推动作用(Brandt 等, 1999), 对研究内波离开波源后的传播与演变过程提供了重要的信息(David, 1999)。因此高分辨率海洋内波表层流速信息的提取具有重要的意义。

目前中国还没有开展SAR海洋内波表层流速信息反演的工作。国际上, Brandt 等(1999)首先提出了利用内波剖面的归一化后向散射强度(Normalized Radar Cross Section, NRCS, $\sigma^0$)反演内波参数的可行性。David(1999)提出了利用 Levenberg-Marquardt 最小二乘法, 通过二尺度模型仿真内波的海面后向散射强度来逼近辐射定标后的 SAR 图像内波剖面, 对内波表层流峰值信息进行了反演, 其反演误差在 15%范围内, 这些方法对雷达海面成像模型提出了较高的要求。目前, 利用雷达海面成像模型和 SAR 图像的内波剖面联合反演内波参数还处于探索阶段。

本文基于海洋内波 SAR 成像机理与 M4S 海面微波成像模型, 提出了内波表层流反演的新方法。利用该方法对中国南海海域 3 景 SAR 图像进行内波表层流的反演, 利用仿真内波剖面的海面后向散射强度和实际剖面信号的接近程度评价该方法的收敛性与可行性。

## 2 海洋内波 SAR 成像机理

SAR 海洋内波成像的前提是内波在波源产生、

**收稿日期**: 2008-08-22; **修订日期**: 2008-11-18

**第一作者简介**: 范开国(1981— ), 男, 博士, 目前主要从事卫星海洋遥感和大气遥感的研究工作。已发表学术论文 15 篇。E-mail: van.fkg@tom.com。

传播与演变的过程中，在海表层形成的辐聚或辐散变化的表层流场与风致海表面微尺度波的产生(Alpers, 1985)。研究结果表明(Alpers, 1985; Thomson & Gasparovic, 1986)，在2—9m/s的中等风速条件下，SAR 可以探测到海洋内波。

微波穿透海水的深度仅为厘米量级，SAR 不能直接观测到水下数十米，甚至数百米深处的海洋内波，SAR 观测到的是海面后向散射强度。海洋内波之所以被SAR观测到是由于海洋内波间接改变了海面后向散射强度。

实验和研究结果表明，海洋内波 SAR 成像机理由 3 个物理过程组成(Alpers & Hennings, 1984; Alpers, 1985; Thomson & Gasparovic, 1986)：(1) 海洋内波引起海表层流场的变化，使表层流场发生辐聚或辐散；(2) 变化的表层流场与海表面风致微尺度波相互作用，改变海表面微尺度波的空间分布；(3) 雷达波与海表面微尺度波的相互作用，该过程决定海面后向散射强度。

## 3 M4S 海面微波成像模型

M4S 是德国科学家 Romeiser 自 1994 年来开发的海面微波成像模型，其基本构成包括两部分：作用量谱平衡方程的求解和海面微波仿真成像。

### 3.1 作用量谱平衡方程

海洋内波的表层流对海面微尺度波的调制可以用 Wentzel-Kramers-Brillouin 弱相互作用理论描述(Alpers, 1984; Romeiser & Alpers, 1997)。根据这个理论，缓慢变化流场中的定常微尺度波能谱密度的变化满足作用量谱平衡方程(Action Balance Equation):

$$\frac{\mathrm{d}A}{\mathrm{d}t}=\frac{\partial\Omega}{\partial k_x}\frac{\partial A}{\partial x}+\frac{\partial\Omega}{\partial k_y}\frac{\partial A}{\partial y}-\frac{\partial\Omega}{\partial x}\frac{\partial A}{\partial k_x}-\frac{\partial\Omega}{\partial y}\frac{\partial A}{\partial k_y}=S \quad (1)$$

其中 $A(\boldsymbol{r}, \boldsymbol{k}, t)$为作用量谱，$\Omega(\boldsymbol{r}, \boldsymbol{k}, t)$为视频率，$\boldsymbol{r} = (x, y)$为空间变量，$\boldsymbol{k}=(k_x, k_y)$为微尺度波波数，$S(\boldsymbol{r}, \boldsymbol{k}, t)$为源函数，表征微尺度波能量增加和耗散过程。在 M4S 模型程序库里，通过射线追踪的数值积分方法求解作用量谱平衡方程，计算给定表流场和风场下的海表面微尺度波谱。

### 3.2 海面微波仿真成像

在 Bragg 共振散射理论的基础上，Romeiser 和 Alpers 等(1997)提出了一种改进的组合表面模式(Improved Composite Surface Model)仿真粗糙海面的微波散射成像。这种散射模式从某种意义上也是三尺度模式，即把海面微尺度波分成长波、中波和短波 3 个部分，同时考虑长波和中波对短波的倾斜调制和水动力调制。该模型在理论和试验研究上均体现了对海面微波散射成像的实际情况(Romeiser 等, 1994; Romeiser & Alpers, 1997)。根据海表面微尺度波谱和雷达参数，利用 M4S 模型程序仿真海面后向散射强度。

## 4 反演流程

Alpers 与 Hennings 指出，在线性近似下，SAR 内波海面后向散射强度的相对变化与内波表层流速的关系为(Hughes 1978; Alpers & Hennings, 1984):

$$\frac{\Delta\sigma^0}{\sigma_0^0}=-A\cos^2\phi\frac{\partial U_x}{\partial x}=-C\frac{\partial U_x}{\partial x} \quad (2)$$

其中，$\Delta\sigma^0=\sigma^0-\sigma_0^0$，$\sigma^0$ 为海洋内波雷达海面后向散射强度，$\sigma_0^0$ 为背景海面的雷达后向散射强度，$A$ 是与风速、风向等因素相关的系数，$\phi$为雷达视向到内波传播方向的夹角，$C=A\cos^2\phi$。从式(2)看出，海面后向散射强度的相对变化与流速梯度成正比，借助海面后向散射强度的相对变化估算流速梯度。

对于海洋内波表层流，根据模式流场的数据设定远离前导波区域的流速，通过积分方法获得猜测流速，构造初始猜测流场。通过 M4S 模型仿真海洋内波的 SAR 海面后向散射强度，利用二分法不断地修改风速和内波剖面上的流速梯度，使仿真结果最大程度的逼近实际SAR图像上的海面后向散射强度，输出最终风速、表层流速等参数，其中初始风速和流速梯度的合适选择会加快迭代仿真的收敛速度。图 1 给出了上述过程的流程图。

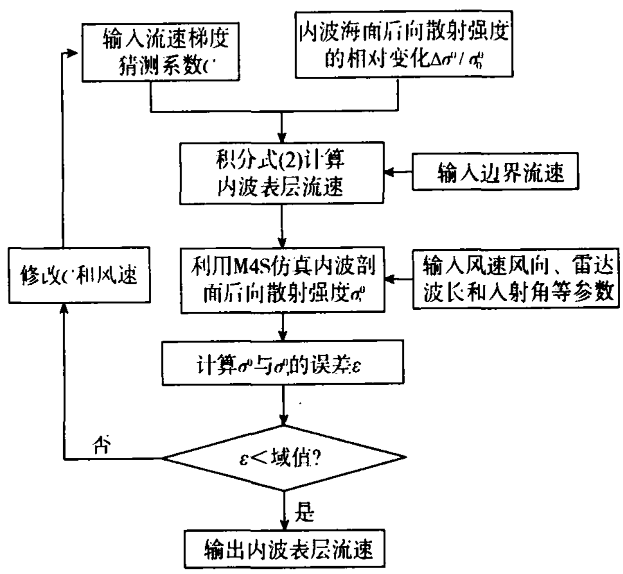


图 1 基于 M4S 模型的 SAR 海洋内波表层流反演流程

## 5 反演结果

### 5.1 实例一

图 2(a)为成像于 2000-10-02 10 时(BJT), 东沙岛西北部海域的 ERS-2 SAR 图像, 分辨率为 12.5m。选取图 2(a)中的 *A*—*B* 剖面, 图 2(b)实线。根据雷达数据得到入射角为 20.15°, 雷达波长为 5.66cm。在一定的时间范围内一幅宽幅为 100 km$^2$的 SAR 图像中, 可以模式的风向资料来逼近 SAR 成像时刻的风向, 但风速变化会有几米到十几米的量级。因此, 可以从 NCEP 数据获得风向信息, 利用迭代仿真的方式对辐射定标后的 SAR 图像进行风速反演。

根据日平均 NCEP 分析资料得出当天 SAR 成像在该海域的风向约为 68.46°, 风速约为 2.77m/s。根据 NCEP 分析风速、风向资料和线性关系初步计算得到初始梯度放大因子 *C* 为 0.0007, 利用图 1 的流程进行迭代反演。经过 17 步迭代后, 输出最终风速大小为 1.29m/s, 梯度放大因子 *C* 为 0.000282。图 2(c)为反演得到的表层流速, 最终仿真的海面后向散射强度如图 2(b)虚线所示, 与实际海洋内波 SAR 图像信号间的相关系数达到 92.3%。

### 5.2 实例二

图 3(a)所示的 SAR 图像是 1998-06-23 22 时(BJT), 东沙岛附近海域的 ERS-2 图像, 该图像的分辨率是 12.5m。选取图 3(a)中的 *M*—*N* 剖面, 如图 3(b)实线所示。读取雷达数据得到入射角为 21.65°, 雷达波长为 5.66cm, 根据 NCEP 再分析资料获得该区域的风速为 1.98m/s, 风向为 150.75°。设初始梯度放大因子 *C* 为 0.0007, 利用图 1 的流程经过 10 步迭代后, 输出最终风速大小为 2.15m/s, 梯度放大因子 *C* 为 0.000888。图 3(c)为反演得到的表层流速。最终仿真的海面后向散射强度如图 3(b)虚线所示, 与实际海洋内波的海面后向散射强度之间的相关系数达到 93.8%。

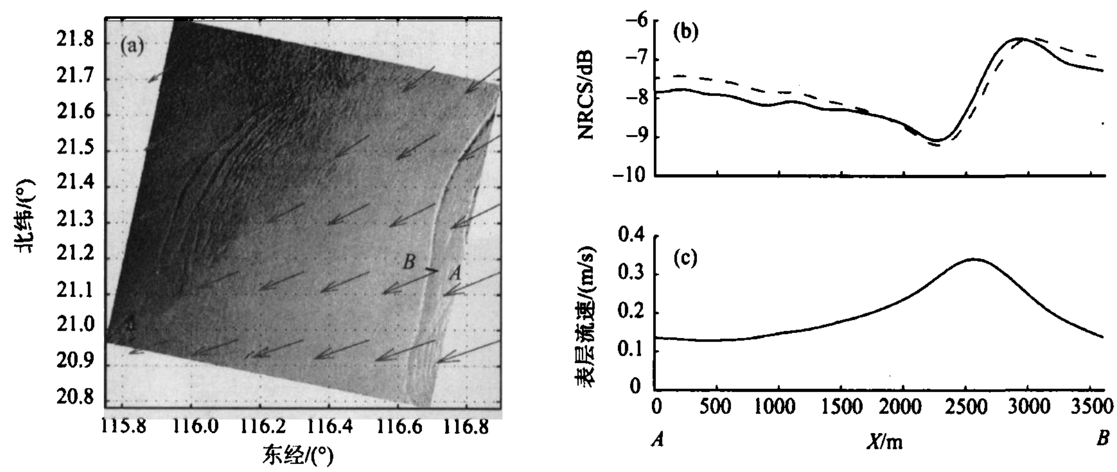


图 2 (a) 2000-10-02 10 时的 ERS-2 SAR 图像与 NCEP 插值风场(箭头); (b) *A*—*B* 剖面的海面后向散射强度(实线)和仿真的海面后向散射强度(虚线); (c) 反演的表层流速

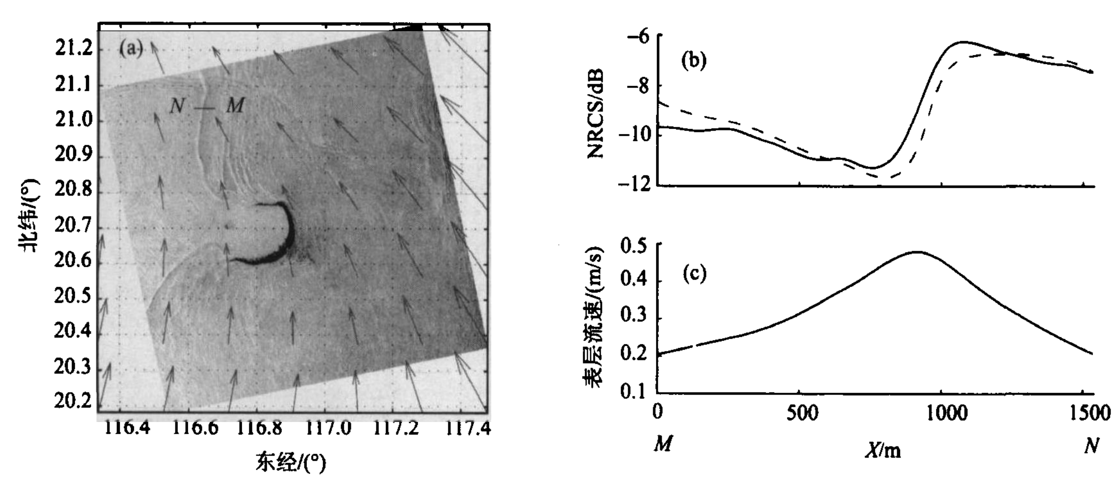


图 3 (a) 1998-06-23 22 时的 ERS-2 SAR 图像与 NCEP 插值风场(箭头); (b) *M*—*N* 剖面的后向散射强度(实线)和仿真的后向散射强度(虚线); (c) 反演的表层流速

### 5.3 实例三

图 4(a)所示的SAR图像为成像于1998-04-22 10时(BJT)，分辨率为 12.5m 的东沙岛附近海域的ERS-2图像。选取图 4(a)中的 $P—Q$ 剖面，如图 4(b)实线。其中入射角为 26.35°，雷达波长为 5.66cm，根据 NCEP 再分析资料获得该区域的风速为 2.36m/s，风向为 149.67°。初始梯度放大因子 $C$ 设为 0.0007，经过15步迭代反演后，输出最终风速为1.92m/s，梯度放大因子 $C$ 为 0.000356，最终仿真的海面后向散射强度如图 4(b)虚线所示，两者相关系数达到 95.8%，图 4(c)为反演得到的表层流速。

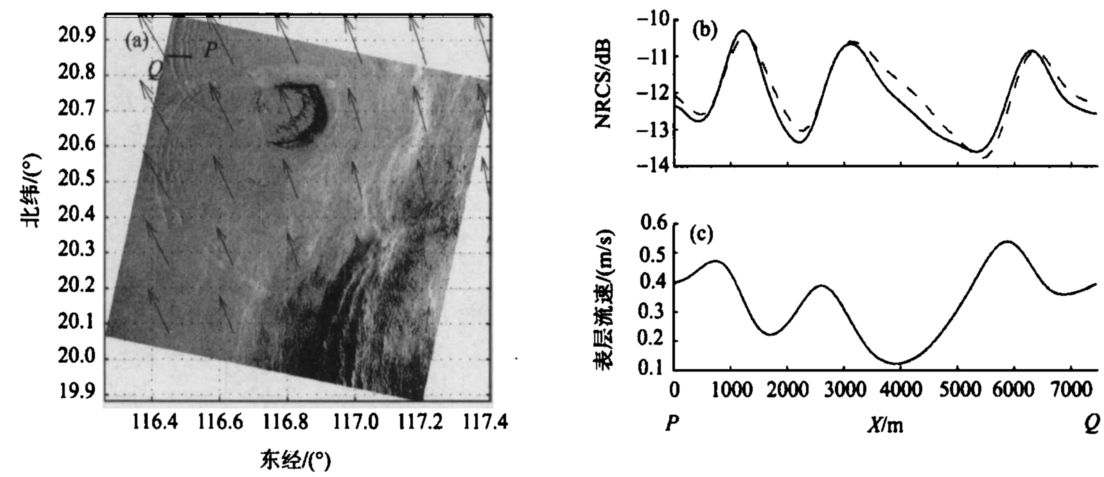


图 4 (a) 1998-04-22 10时的 ERS-2 SAR 图像与 NCEP 插值风场(箭头); (b) $P—Q$ 剖面的后向散射强度(实线)和仿真的后向散射强度(虚线); (c) 反演的表层流速

## 6 结论

根据海洋内波SAR成像机理与M4S海面微波成像模型，建立了 SAR 海洋内波表层流反演的新方法，该方法的收敛性与可行性通过仿真内波剖面的海面后向散射强度和实际剖面信号的接近程度进行评价。

利用该方法对东沙岛附近的海洋内波实例进行研究，结果表明，仿真的海面后向散射强度结果和实际内波剖面的信号非常吻合，相关系数达到 90%以上，说明利用该方法进行 SAR 海洋内波表层流反演是收敛、可行的。此外，该方法不需要对海洋内波动力学模式进行假定，对任何水深和任何层化条件下的海洋内波适用，对 SAR 海洋内波参数反演方法是有益增补。未来需要通过获取海上同步观测数据，给出远离前导波区域准确的初始流速，同时对表层流反演精度进行了有效评估。

**致 谢** 感谢德国汉堡大学海洋遥感中心 Romeiser 博士提供 M4S 程序，中国科学院大气物理研究所提供 NCEP 气象数据，中国科学院遥感卫星地面站和欧洲空间局提供的 SAR 卫星数据。

## REFERENCES

Alpers W and Hennings I. 1984. A theory of the imaging mechanism of underwater bottom topography by real and synthetic aperture radar. *Journal of Geophysical Research*, **89**: 10529—10546

Alpers W. 1985. Theory of radar imaging of internal waves. *Nature*, **314**: 245—247

Brandt P, Romeiser R and Rubino A. 1999. On the determination of characteristics of the interior ocean dynamics from radar signatures of internal solitary waves. *Journal of Geophysical Research*, **104**(C12): 30039—30045

Cai S Q, Long X M and Gan Z J. 2003. A method to estimate the forces exerted by internal solitons on cylindrical piles. *Ocean Engineering*, **30**: 673—689

David Y L. 1999. Extraction of surface currents of solitary internal waves from synthetic aperture radar data. Proceedings of the IEEE Sixth Working Conference on Current Measurement. San Diego: IEEE

Hughes B A. 1978. The effect of internal waves on surface wind waves 2. Theoretical analysis. *Journal of Geophysical Research*, **102**: 1163—1181

Romeiser R and Alpers W. 1997. An improved composite surface model for the radar backscattering cross section of the ocean surface 1. Theory of the model and optimization/validation by scatterometer Data. *Journal of Geophysical Research*, **102**: 25238—25250

Romeiser R and Alpers W. 1997. An improved composite surface model for the radar backscattering cross section of the ocean surface 2. Model response to surface roughness variations and the radar imaging of underwater bottom topography. *Journal of Geophysical Research*, **102**(C11): 25 251—25 267

Romeiser R, Schnidt A and Alpers W. 1994. A three-scale composite surface model for the ocean wave-radar modulation transfer function. *Journal of Geophysical Research*, **99**(C5): 9785—9801

Thomson R E and Gasparovic R F. 1986. Intensity modulation in SAR image of internal waves. *Nature*, **320**(14): 345—348